In-gas-jet laser spectroscopy of ^{254}No with JetRIS

Jeremy Lantis,[1,2,*] Arno Claessens,[3] Danny Münzberg,[1,2,4] Julian Auler,[1] Michael Block,[1,2,4] Premaditya Chhetri,[3] Christoph E. Düllmann,[1,2,4] Rafael Ferrer,[3] Francesca Giacoppo,[4] Manuel J. Gutiérrez,[2,4] Fedor Ivandikov,[3] Oliver Kaleja,[5] Tom Kieck,[2,4] EunKang Kim,[1] Mustapha Laatiaoui,[1,2,4] Nathalie Lecesne,[6] Vladimir Manea,[7] Steven Nothhelfer,[1,2,4] Sebastian Raeder,[2,4] Jekabs Romans,[3] Elisa Romero-Romero,[1,2] Antoine de Roubin,[3] Hervé Savajols,[6] Simon Sels,[3] Matou Stemmler,[1] Piet Van Duppen,[3] Thomas Walther,[8] Jessica Warbinek,[1,2,4] Klaus Wendt,[1] Alexander Yakushev,[4] and Alexandra Zadvornaya[9]

[1]*Johannes Gutenberg-Universität Mainz, 55099 Mainz, Germany*
[2]*Helmholtz-Institut Mainz, 55099 Mainz, Germany*
[3]*KU Leuven, Instituut voor Kern- en Stralingsfysica, 3001 Leuven, Belgium*
[4]*GSI Helmholtzzentrum für Schwerionenforschung GmbH, 64291 Darmstadt, Germany*
[5]*Universität Greifswald, 17489 Greifswald, Germany*
[6]*GANIL, CEA/DRF-CNRS/IN2P3, 55027 Caen, France*
[7]*Université Paris-Saclay, CNRS/IN2P3, IJCLab, 91405 Orsay, France*
[8]*Technische Universität Darmstadt, Schlossgartenstraße 7, 64291 Darmstadt, Germany*
[9]*II. Physikalisches Institut, Justus-Liebig-Universität Gießen, 35392 Gießen, Germany*

(Received 6 December 2023; accepted 6 May 2024; published 24 June 2024)

Here we report online results with the in-gas-Jet Resonance Ionization Spectroscopy (JetRIS) apparatus. The $^1S_0 \leftrightarrow {}^1P_1$ transition of ^{254}No was successfully measured with sub-GHz resolution, marking a fivefold improvement over previous measurements. Recent developments in laser spectroscopy have allowed access to more exotic nuclei, but measurements of the heavy actinide region have been limited by line broadening mechanisms, limiting the precision with which nuclear properties can be deduced from the hyperfine spectrum. JetRIS provides a method to measure the heavy actinide region with a high level of sensitivity and higher resolution than previous experiments. The offline and online characterizations of the system are reported, and future perspectives are presented.

DOI: 10.1103/PhysRevResearch.6.023318

I. INTRODUCTION

Laser-spectroscopic methods provide a tool to study the fundamental properties of the atom and its nucleus. Atomic transition energies and their strengths can be determined, providing information about the electronic structure, and accurate determination of ionization potentials is possible. Through the interaction between the atomic electrons and the nucleus, information about the spin, size, and deformation of the ground and isomeric nuclear states can be obtained. Independent of nuclear models, these measurements provide information that is essential to understand the structure of the nucleus. A variety of techniques have been developed to study exotic nuclides at a wide range of masses, and this research has been the topic of multiple reviews in recent years [1–5].

Obtaining atomic and nuclear information in the actinide region is crucial for understanding the fundamental principles of nuclear existence, but it is particularly challenging as these nuclides are located at the regions of the largest proton numbers Z. Among the heavy actinides, most nuclides can only be produced in fusion-evaporation reactions, typically at rates of one per second or lower. These low production rates limit vital information about the electronic structure that is generally determined with stable isotopes for lighter elements. Historically, in-gas-cell laser spectroscopy has been the technique of choice to study short-lived isotopes in this region. Pioneering work was performed on the fission isomers of ^{240,242}Am ($Z = 95$) [6] demonstrating the ability to measure species with rates as low as 10 s^{-1}, followed by the first determination of atomic levels in Fm ($Z = 100$) [7]. More recent examples include the measurement of the chain of $^{212-215}$Ac [8], which revealed the influence of the unpaired $\pi h_{9/2}$ proton on the nuclear structure of the region. Even with these developments, the *trans*-fermium region remained out of reach for existing in-gas-cell laser spectroscopy facilities until advances were made using the RAdioactive Decay detected Resonance Ionization Spectroscopy technique [9,10,12]. The RADRIS technique was used to determine the first atomic transition in No ($Z = 102$) [11], providing an avenue to probe relativistic effects in the atomic structure of this region.

*Present address: Physics Division, Argonne National Laboratory, Lemont, IL 60439, USA.

Further experiments provided the first precision measurement of the ionization potential of nobelium [14], and determination of the ground-state nuclear properties of a chain of nobelium isotopes [13].

Although highly sensitive, the RADRIS technique has limitations that restrict the elements and isotopes that can be studied. One limiting factor is the lifetime of the species of interest, as time-consuming steps between the collection and subsequent measurement reduce the overall efficiency of the technique for short-lived isotopes ($T_{1/2} < 1$ s). Recent work has been performed to minimize these delays, as described in Ref. [15]. The second limiting factor, and the focus of this work, is the achievable spectral resolution. As in-gas-cell laser spectroscopy is performed in a high-pressure environment at room temperature, pressure and Doppler broadening of the spectral lines lead to a spectral resolution of about 4 GHz, in turn limiting access to nuclear properties and the precision with which they can be extracted from hyperfine spectra.

Developments at the Leuven Isotope Separator On Line (LISOL) facility resulted in the first online experiment of laser spectroscopy in a supersonic gas jet [16–18]. The supersonic gas-jet was formed using a convergent-divergent (de Laval) nozzle, where the gas traveling through the nozzle progresses from subsonic velocities to supersonic as the gas expands in the downstream divergent section of the nozzle. The gas moves uniformly in the jet and can be characterized by the Mach number (M), defined as the ratio of the stream velocity (u) to the local speed of sound (a), which are dependent on the choice of buffer gas and the conditions in the gas cell, as can be seen in Eqs. (1) and (2) below,

$$a = \sqrt{\frac{\gamma k T}{m}}, \tag{1}$$

$$u = \sqrt{\frac{\gamma k T_0 M^2}{m\left(1 + \left[\frac{\gamma-1}{2}\right]M^2\right)}}, \tag{2}$$

where γ is the adiabatic index, or the ratio of the heat capacity at constant pressure to heat capacity at constant volume, of the buffer gas, and is equal to 5/3 for monatomic gases like argon. k is the Boltzmann constant, m is the mass of the buffer gas atom, T is the temperature in the gas jet, and T_0 is the stagnation temperature, or the temperature of the buffer gas in the cell before expansion. As the Mach number increases, it quickly and asymptotically approaches a maximum stream velocity, approximately 558 m/s in the case of argon, as the local speed of sound continues to drop. The temperature and density of the gas-jet are inversely related to the square of the Mach number, as can be seen in Eqs. (3) and (4),

$$T = \frac{T_0}{1 + \left[\frac{\gamma-1}{2}\right]M^2}, \tag{3}$$

$$P = P_0\left(1 + \frac{\gamma - 1}{2}M^2\right)^{\frac{-\gamma}{\gamma-1}}. \tag{4}$$

At $M = 7$, the temperature in the gas-jet is reduced to 17 K and the pressure and density reach 5% of the stagnation conditions. This large reduction allows for a large gain in the spectral resolution over the in-gas-cell laser spectroscopy method, where Doppler and pressure broadening effects dominate the spectral line shape. Critically the developments at the LISOL facility demonstrated that the in-gas-jet laser spectroscopy technique could maintain the total efficiency of the in-gas-cell method while achieving an order of magnitude improvement in the spectral resolution. This presents in-gas-jet laser spectroscopy as a powerful tool for studying rare nuclei with production rates that prevent their study by other techniques such as collinear laser spectroscopy.

The concept of the JetRIS apparatus was introduced in Ref. [19] as a method to study the heaviest elements with the in-gas-jet laser spectroscopy method. JetRIS combines the use of filament neutralization from RADRIS with the in-gas-jet ionization technique to achieve both a high efficiency and high spectral resolution. This article presents the status of the JetRIS apparatus, including offline studies for characterization, online results, and the outlook for future measurements. These comprise the design and characterization of a hypersonic nozzle by resonance ionization spectroscopy flow mapping of copper isotopes seeded in an argon gas jet, and by laser-induced fluorescence measurements of stable dysprosium samples [20]. Radioactive recoil-ion sources were also used to determine the overall efficiency of the system. These offline measurements resulted in improvements in performance that allowed successful laser spectroscopy measurements of ^{254}No.

II. EXPERIMENT

A. JetRIS apparatus

The concept of the JetRIS apparatus was presented in Ref. [19]. Here we briefly repeat its concept and main characteristics. The JetRIS apparatus consists of three sections, shown in schematic form in Fig. 1. First, an argon gas cell (80 mbar) is used to thermalize reaction products for online experiments, or as a cell for the production of atoms and ions from offline sources. In online experiments, the isotopes of interest are produced through fusion-evaporation reactions, with the separator for heavy ion products (SHIP) [21,22] used to separate the primary beam from the reaction products. Within the gas cell, a series of dc electrodes is used to guide ions to a thin tantalum filament that is biased to a negative potential. The ions are collected and neutralized on the filament. The ions first are transported through a cylindric electrode structure (dc cage with a field gradient of about 4.2 V/cm) leading to a second set of concentric electrodes with decreasing diameter (dc funnel with a field gradient of 18.5 V/cm) to efficiently guide the ions to the filament, which was held at a potential of −150 V. The filament is resistively heated, producing an atomic vapor that is carried by the laminar flow of the argon buffer gas through a de Laval nozzle into a lower pressure (7×10^{-3} mbar) jet chamber, where the expanding gas forms a collimated, low-temperature rarefied gas jet (see Sec. II B). After laser resonant ionization within the gas jet, the resulting photo ions enter a 90° bent radiofrequency quadrupole (RFQ) ion guide, where they are separated from the remaining atoms and transported through a differential pumping barrier to the detector. Detection can be performed with either a light-insensitive silicon detector for online measurements, as discussed later in Sec. II D, or a channel electron multiplier detector for ion detection of stable isotopes.

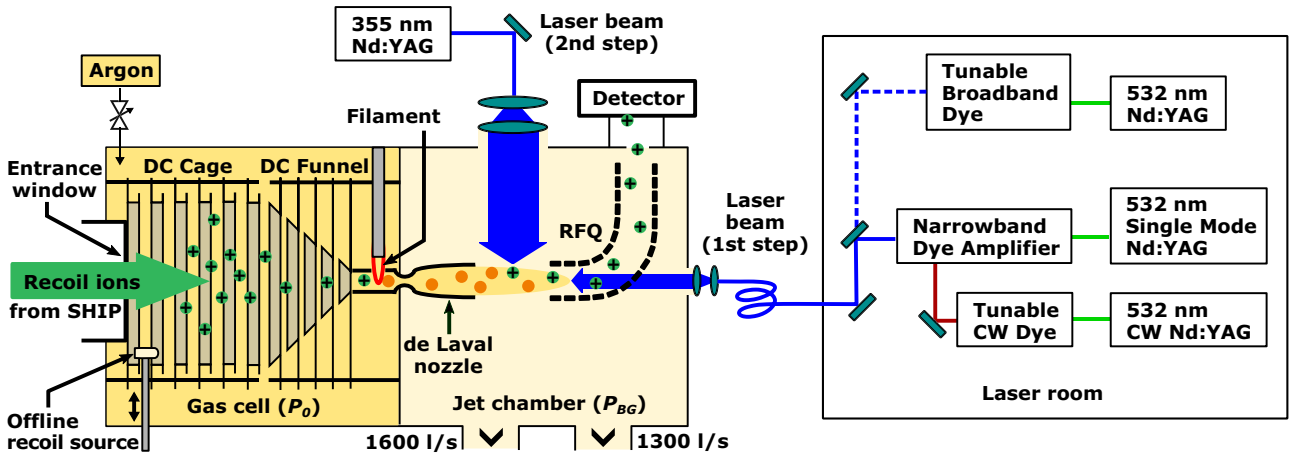

FIG. 1. Schematic layout of the JetRIS apparatus. An 80-mbar high-pressure gas cell is used to thermalize fusion-evaporation reaction products from SHIP, which are transported to and adsorbed onto a heated filament and neutralized for subsequent laser ionization spectroscopy measurements in a gas jet.

B. Hypersonic low-P_0 de Laval nozzle

The in-gas-jet laser ionization and spectroscopy technique relies on a convergent-divergent (de Laval) nozzle to deliver a gas jet with a high Mach number M (i.e., low temperature T) and high flow uniformity (i.e., jet collimation). These properties depend critically on the stagnation pressure P_0 inside the JetRIS gas cell and the background pressure P_{BG} of the environment where the jet forms, referred to henceforth as the jet chamber. A previous design operated at high stagnation pressures ($P_0 = 300$ mbar), suited for gas cells relying on only-gas-flow transportation, was reported in [23] and provided a cold (17 K), highly collimated, and uniform gas jet with a Mach number of 8.1 and a length of 62 mm. For this high-P_0 nozzle it was observed that below a stagnation pressure of 100 mbar the jet formation was inhibited due to a significant thickening of the boundary layer on the nozzle walls [24]. Following the same design prospects, a de Laval nozzle, operational at lower stagnation conditions ($P_0 \leqslant 100$ mbar) and suited for gas cell ion transport using dc fields, was developed for JetRIS.

Contour design and computational fluid dynamics (CFD) calculations of the low P_0 nozzle were performed at the Von Karman Institute for Fluid Dynamics (VKI), Sint-Genesius-Rode, Belgium. Starting from the same inviscid contour as the high-P_0 nozzle, a viscous correction based on the JetRIS operating conditions was applied leading to three significant adjustments. The throat diameter was slightly increased from 1.029 to 1.067 mm for a higher mass flow. The opening angle of the diverging nozzle part was increased from $\omega = 16.6°$ to 28.2°, and the nozzle was shortened from 37.5 to 18.0 mm.

According to the numerical calculations, this design results in the formation of a 60-mm-long gas jet with a core diameter of about 5 mm (cf. Fig. 2), but the simulations also indicate that the hypersonic gas jet is highly sensitive to weak variations in the background pressure. Finally, two low-P_0 nozzles were CNC-machined out of brass (MS58) to within a contour error of less than 5 µm and a surface roughness of 0.1 µm. The nozzle as well as the contour deviation of the divergent nozzle part are shown in Fig. 3. The surface roughness was measured at three different positions by first casting a negative replica and then measuring with an optical profilometer (Sensofar Neox). For all three points, roughness is found to be between 90 and 110 nm. Initial characterization measurements to gauge the gas jet properties were performed at the IGLIS laboratory [16] at KU Leuven using

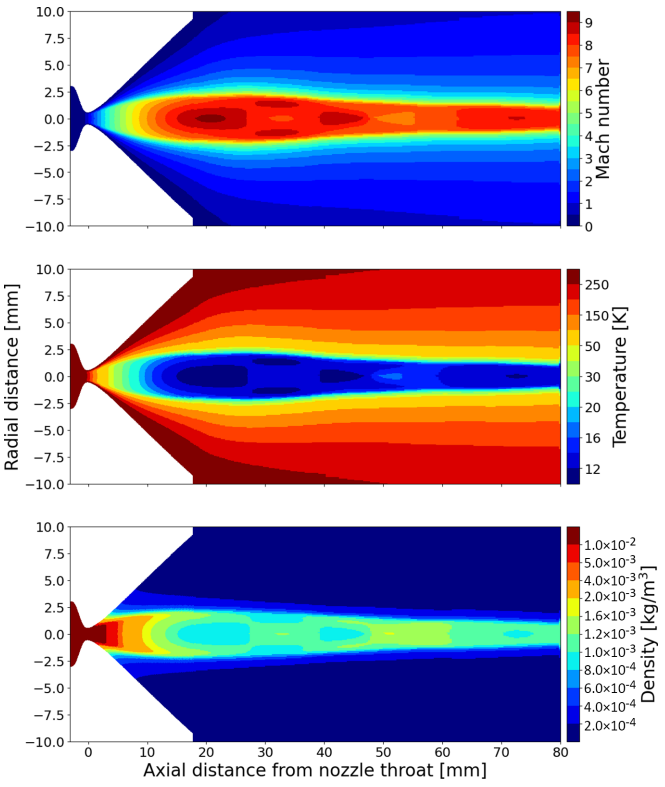

FIG. 2. 2D plot of the Mach number, temperature, and mass density distributions as calculated by the VKI HYPNOZE design code. The pumping capacity of JetRIS allows only for nozzle throat diameters of about 1 mm using stagnation conditions of $P_0 = 80$ mbar and $T_0 = 300$ K.

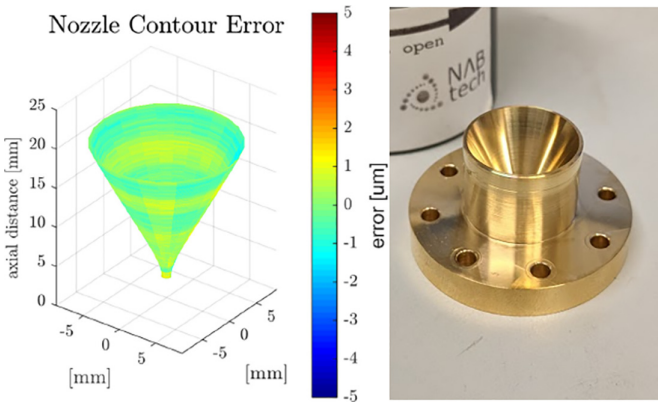

FIG. 3. Picture of the brass low-P_0 nozzle (right) with a 3D-visualization of the contour error (left). The error is the contour deviation between machined and calculated contour and is measured with a Werth HA 400 CMM machine in combination with a Fiber-Probe for more than 55 000 points.

planar laser-induced fluorescence (PLIF) measurements [25] on ^{63}Cu. Surprisingly, a poor flow uniformity was observed at the designed background pressure of 2.5×10^{-2} mbar. Lowering the background pressure hinted towards an improved uniformity, but this could not be ascertained by PLIF. These investigations were complemented by PLIF measurements of ^{164}Dy using the second contoured nozzle, for which the results are discussed in [20]. To address the uncertainty in the uniformity of the gas jet, additional characterization was performed using resonance ionization spectroscopy (RIS) flow mapping at the gas-jet core with ^{63}Cu, as described in [23]. RIS flow mapping is achieved by high-resolution laser spectroscopy where a narrowband scanning laser is aligned along the axis of the gas jet, and the ionization laser is aligned in a transverse manner, such that photoions are only produced in the well-defined region where the lasers overlap. The ionization laser was moved to across the gas jet, allowing regions to be investigated separately. A partial scan of the hyperfine structure (the low-energy doublet) of ^{63}Cu was then measured and the spectra were fitted using χ^2 minimization of a Voigt profile containing two peaks. The Doppler shift of the centroid and the Gaussian width at half-maximum of the peaks are extracted from the spectra, from which the stagnation temperature of the gas inside the gas cell T_0 and the local gas jet temperature T are determined. These measurements were conducted at four different background pressures starting from the designed conditions (2.5×10^{-2} mbar) to the lowest achievable pressure (5.9×10^{-3} mbar) in order to obtain the ideal flow match conditions. The resulting Mach numbers and densities are shown in Fig. 4.

A significant deviation is found between the calculated behavior of the Mach number and the RIS flow mapping results. A high-Mach-number core was observed in the gas jet with flow-matching conditions at much lower background pressures than initially anticipated, with a background pressure of 7×10^{-3} mbar, and subsequently the operational vacuum conditions for our measurements were fixed to this value.

The need for a lower background pressure to obtain a homogeneous gas jet with a high Mach number points to an

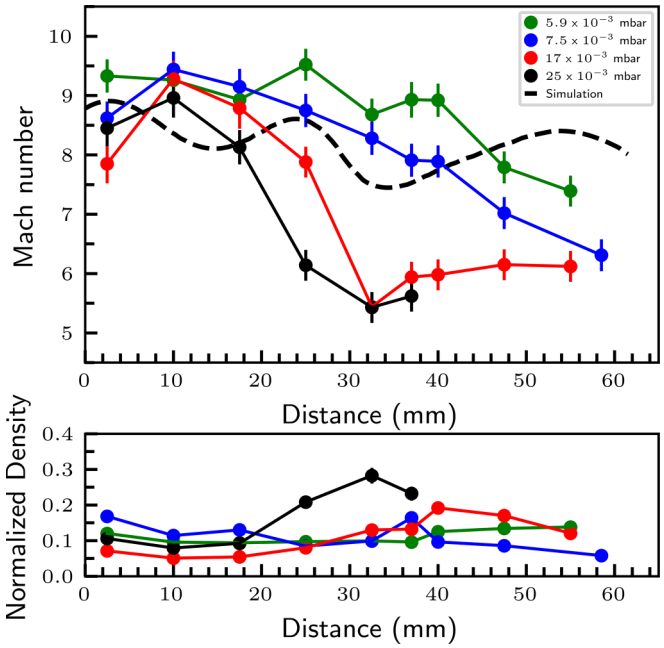

FIG. 4. The measured Mach number distribution (top) and density distribution (bottom) along the jet core for $P_0 = 80$ mbar and different background pressures. The calculated Mach number along the gas jet is shown as a dashed line.

overestimation of the static pressure (the pressure inside the jet) in the CFD calculations. A mismatch in static pressure at the exit plane (P_E) and background pressure leads to a radial velocity component after crossing the nozzle exit plane, resulting in expansion-contraction cycles in the gas jet that inhibit proper jet formation. The boundary layer between the nozzle and jet core is of critical importance in hypersonic flow, and disturbances here propagate through the entire core. Due to the large mean free path in rarefied gasses, it is possible that the boundary condition of $v = 0$ is no longer met. The resulting slip flow regime leads to higher average velocities in the boundary layer, reducing the exit static pressure (P_e). This deviation from the Navier-Stokes equation is not accounted for in the CFD calculations.

C. Online laser system

The in-gas-jet method requires a state-of-the-art laser system to provide high power and short (∼10 ns) pulses at a high-repetition rate to maximize the laser ionization efficiency, while also providing narrow-bandwidth light for high-resolution laser spectroscopy in the cold gas jet. A pulse repetition rate of 15 kHz is ideal to irradiate every atom at least once within the first 40 mm of the gas jet, as the flow velocity is about 550 ms^{-1} at $T_0 = 300$ K.

As a two-step ionization scheme was used, multiple lasers were used in this experiment. These can be grouped into a narrowband and a broadband system. A schematic drawing of the systems can be seen in Fig. 1. The narrowband laser system is comprised of a pulse dye amplifier system (PDA) seeded by a tunable, single-mode continuous-wave (CW) dye laser, which was used for the first excitation step, and the direct light from a high-power Nd:YAG laser provided

the nonresonant ionization step. To maximize ionization efficiency in these experiments, the scanning laser should have sufficient bandwidth to cover the full thermal distribution of nobelium atoms in the gas jet. For this particular nozzle, this would imply a bandwidth of 160 MHz ($T_0 = 330$ K). The two-stage PDA is seeded by a wavelength tunable CW dye laser (Matisse, Sirah Lasertechnik) and optically pumped by a state-of-the-art single longitudinal mode Nd:YAG laser (Edgewave, PXn300-2-GF-SLM). This laser can provide up to 60 W of 532 nm light in Fourier-limited pulses of about 8 ns at repetition rates of 15 kHz. Single-mode operation of the laser was used to avoid resonances caused by additional modes that are typically present in high-repetition-rate PDA pumped Nd:YAG lasers [26]. The resulting pulses from the PDA when equipped with the laser dye 4-Dicyanomethylene-2-methyl-6-p-dimethylaminostyryl-4H-pyran (DCM) in a mixture of dimethyl sulfoxide (DMSO) and ethanol (75% and 25%) give a pulse width of about 4.5 ns and a bandwidth of 95 MHz in fundamental light. By frequency doubling with a single-pass second-harmonic generation (SHG) unit using a β-barium borate (BBO) crystal, the pulses are shortened to about 3 ns resulting in a spectral bandwidth of 150 MHz. A detailed characterization of the narrowband PDA using a prototype Nd:YAG at repetition rates of 10 kHz is reported in Ref. [26].

In addition, a broadband laser system was used during preparatory online studies using ^{155}Yb to ensure gas jet formation and good operation of the JetRIS apparatus. The laser light for the first excitation step was produced with a pulsed dye laser (Sirah Lasertechnik, Credo) pumped by a multimode Nd:YAG laser (Edgewave, InnoSlab IS400-2-L) for which the repetition rate is limited to 10 kHz and the bandwidth is limited by the laser grating to approximately 1.8 GHz.

The ionization step of both laser schemes was realized with the third harmonic of a high-power Nd:YAG laser (Edgewave, InnoSlab IS400-2-L) operated at 10 or 15 kHz for ytterbium or nobelium ionization, providing up to 30 W of UV light.

D. Detector setup

In the online operation of the JetRIS setup, different radioactive isotopes are distinguished by measuring their specific α-decay energy. The decay was measured with a light-insensitive silicon (Mirion PIPS®) detector in an independently-pumped vacuum chamber, separated from the jet chamber by a 2.6-mm-diam pinhole to maintain ultrahigh vacuum. This allows the detector to be set on a potential of -2 kV relative to the nozzle. The acceleration of the ions causes them to be implanted a few nm into the protective layer of the detector and prevents volatile species from desorbing from the surface before decay.

A schematic of the electronics used for the detector is shown in Fig. 5. To maintain a low noise and high resolution α-energy measurement while on high voltage, the -2 kV potential was applied to the entire signal processing chain. The measurement system consists of the previously mentioned silicon detector with 600 mm^2 sensitive surface area, 40 V detector-bias power supply, a preamplifier, and a Red-Pitaya STEMlab 125-14 for digitization. The different supply voltages were generated by a self-designed small-form-factor toroidal transformer to protect the measurement electronics

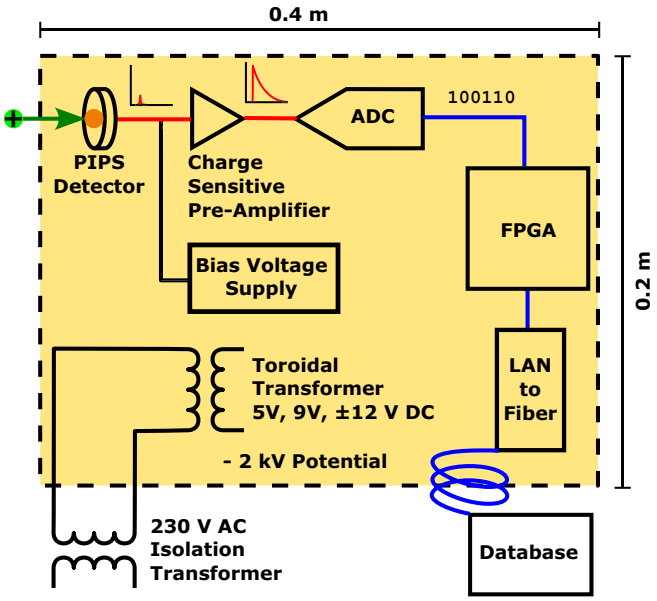

FIG. 5. Schematic of the detector setup to measure the characteristic α-decay of volatile recoil ions. The details are described in the text.

from high-frequency noise of switching power supplies. An isolating transformer was used to decouple the main voltage from the ground potential, and a LAN-to-fiber converter was used to write the single-event decay energy with an 8 ns precision time stamp to a database. Correlation of the measured decays to the laser wavelength was done with the time stamp.

The detector was used through the online experiment to identify various nuclei produced in the production and decay chains of ^{155}Yb, ^{254}No, as well as ^{219}Ra emitted from a recoil source of ^{223}Ra, with a resolution of approximately 80 keV; cf. Fig. 6.

III. OFFLINE CHARACTERIZATION

Characterization of the JetRIS apparatus in offline measurements was carried out to optimize its operation. Offline measurements were performed with radioactive ^{223}Ra recoil sources to characterize the transport of ions through JetRIS, similar to the studies for the cryogenic gas cell used at SHIPTRAP [27]. The overall transport efficiency and speed were measured using these methods.

A. Transport efficiency

The transport efficiency from the gas stopping cell to the detector was investigated as one component of the overall efficiency. A recoil ion source was mounted on a movable rod within the gas cell, and the transport efficiency was determined through the ratio of α-decays detected in the PIPS detector to the known rate of daughter nuclei emitted from the source. Two short-lived species can be observed in the ^{223}Ra decay chain, ^{219}Rn ($t_{\frac{1}{2}} = 3.94$ s) itself as well as ^{215}Po ($t_{\frac{1}{2}} = 1.78$ ms), and the overall transport efficiency was calculated from the observed decays of both species. Based on the geometry of the detector, it was assumed that the detection

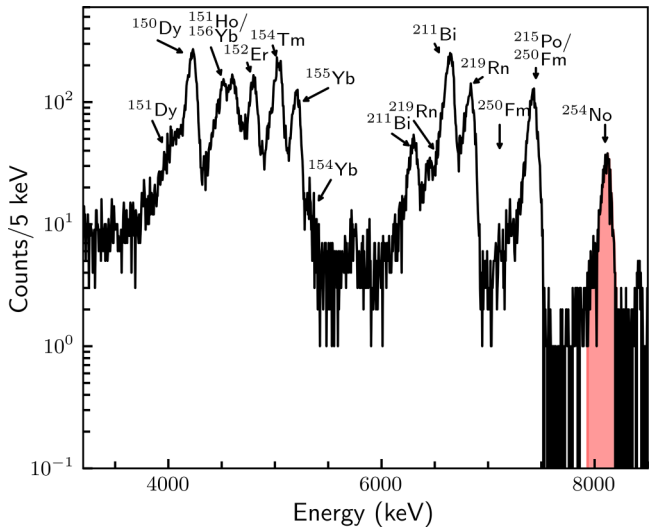

FIG. 6. Alpha spectrum of the nuclei observed during the online experiment using the silicon detector at high voltage as described in the text. The decay chains of ^{155}Yb, ^{254}No, and ^{223}Ra are shown. The red shading indicates the energy gate used for cutting the data on ^{254}No.

efficiency of the implanted recoil ions was 50% with a further 50% reduction in the detected ^{215}Po from recoiled ions leaving the surface of the detector. The rate of recoils from the source was determined by measuring the activity in vacuum with the source positioned at different distances from the detector. The transport efficiency of the ions as a function of distance from the nozzle is shown in Fig. 7.

The source was mounted to a thin tantalum disk used to shield the recoils from the grounded rear flange of the gas cell. The potential of the recoil source and the disk was matched to the potentials applied to the surrounding electrodes. A sharp decrease in transport efficiency was observed when varying the applied voltage away from the local potential. The recoil source was moved along the central axis of the gas cell, providing a map of the transport efficiency for ions that were stopped in different regions of the gas cell. The transport efficiency fell as the recoil source was pulled farther from the de Laval nozzle, as shown in Fig. 7, indicating that significant losses occur in the transport through the cell.

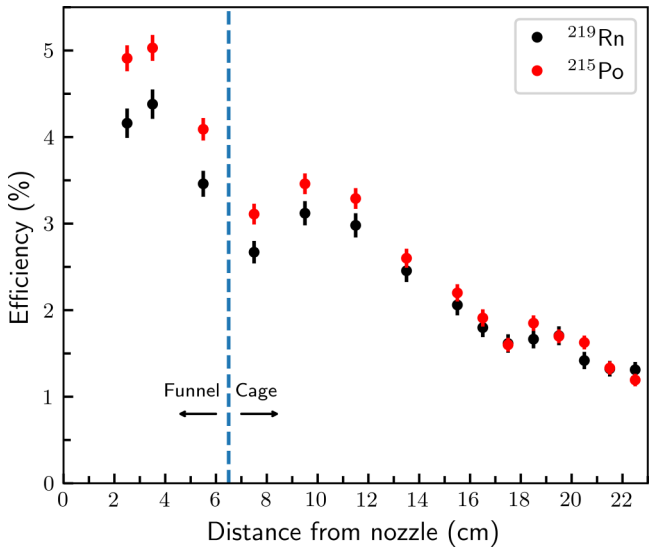

FIG. 7. Offline transport efficiency of the ^{219}Rn and ^{215}Po daughters of a ^{223}Ra recoil source as a function of source distance from the nozzle. The recoil source was mounted on an adjustable rod following the central axis of the JetRIS gas cell.

The initial design of JetRIS featured a gas cell pressure of 30 mbar. Simulations of the distribution of heavy ions in the gas cell at 30 mbar were performed and described in [19]. The most probable stopping distance was located 21 cm from the nozzle. As the gas cell was operated at a higher pressure of 80 mbar during these measurements, it is assumed that the actual stopping distance was located further from the nozzle. Comparing the simulated most probable stopping distance to the measured transport efficiency along the central axis, a transport efficiency of approximately 1.5% can be expected for online measurements.

It should be noted that most transport losses occur within the gas cell, including the transport through the nozzle. The transport efficiencies through the bent RFQ and into the detector cell were investigated by measuring the current of photoions in an offline setting. Here, the investigated electrode was negatively biased by a battery box with 45 V, while the positive terminal was connected to a picoamperemeter (Keithley 6485). A natural ytterbium atom source was resistively heated next to the nozzle, producing a vapor. Two lasers propagating through the nozzle were used to resonantly ionize the atoms, which were carried into the gas jet and to the bent RFQ. Ions impinging on the RFQ rods, connected to the picoamperemeter, led to a measurable current of 20 pA. Afterwards the negative terminal was connected to both transport electrodes inside the detector cell and the measurement was repeated. In this configuration, a current of 15 pA was measured. As a result, a transport efficiency through the bent RFQ and the differential pumping barrier to the detector chamber of 75% was derived.

B. Transport time

Furthermore, the recoil ion source was used to investigate the transport time of ions through the JetRIS apparatus. Cyclic measurements were performed with a period of 500 ms. The floating potential used to prevent the recoil daughters from being attracted back to the source after thermalization and the RF frequency applied to the ion guide to transport ions from the jet to the detection region were pulsed for a short duration (50 ms) with a variable time delay, ΔT, between the pulses. Ions that did not travel from the source to the bent RFQ within this time delay would not be transported to the detector. The count rate as a function of the delay between the pulses of the floating potential and the RFQ was measured and fit to a Gaussian function to determine the mean transport time at different distances from the nozzle in the gas cell, as can be seen in Fig. 8.

Even at the furthest distance of 22.5 cm, a transport time of less than 200 ms was observed. This short time provides access to short-lived species that are currently out of reach for measurements with the RADRIS technique, which even

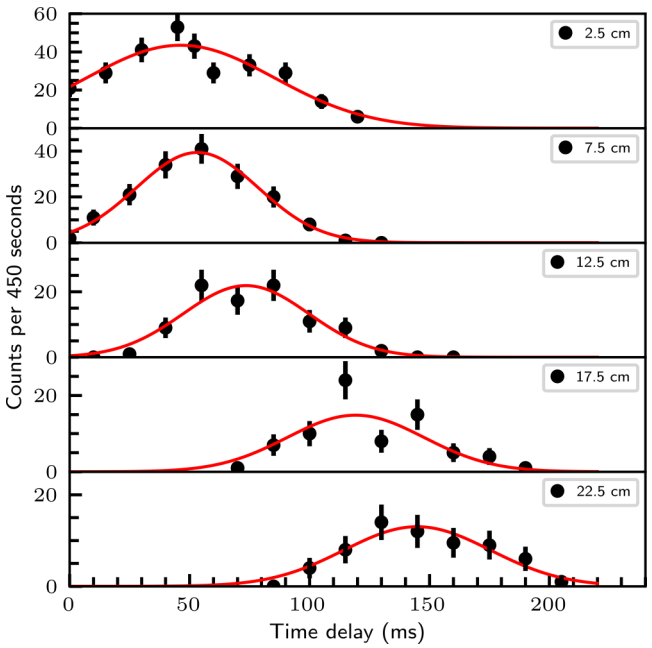

FIG. 8. Effective transport time of recoil ions from the JetRIS gas cell to the detector as a function of distance from the nozzle. The time delay shown is the difference in the rising edges of the potential pulses applied to the recoil source and the bent RFQ.

with recent advancements is limited to species with lifetimes greater than approximately 500 ms [15]. Additionally, a plateau in the transport time was observed as the recoil source approached the nozzle, towards a minimum of approximately 50 ms. Further work is being performed to understand this transport in order to improve the efficiency and to minimize decay losses during transport.

IV. ONLINE EXPERIMENT

The first online experiment using the JetRIS apparatus was performed at the GSI Helmholtzzentrum für Schwerionenforschung in Darmstadt, Germany, targeting ^{254}No and ^{155}Yb. ^{254}No ions were produced through the ^{208}Pb(^{48}Ca, 2n)^{254}No fusion-evaporation reaction, with a cross section of 2 μb [28] at a beam energy of approximately 217 MeV, and ^{155}Yb ions were produced through the ^{112}Sn(^{48}Ca, 2n)^{155}Yb reaction, with a cross section of 7.5 mb [12] at a beam energy of approximately 218 MeV. A beam of ^{48}Ca was accelerated using the UNILAC linear accelerator with average beam currents of up to 0.7 particle ·μA (4×10^{12} particles per second) and impacted on a thin target of approximately 440 μg/cm^2. The target wheel consisted of eight segments. Each segment consisted of about 95% ^{208}Pb and 5% ^{112}Sn, which enables the production of ^{155}Yb and ^{254}No with the same target wheel. ^{155}Yb has been previously used as a diagnostic and calibration measurement with the RADRIS technique, as the overall production rate was approximately 70 times greater than ^{254}No, although the production cross section is more than 1000 times greater [12]. The fusion-evaporation products were separated in flight from the primary beam using SHIP [21,22]. Approximately four ions of ^{254}No per second are available at the entrance of the gas cell with a primary beam intensity of 0.7 particle ·μA. Significant portions of the experiment were conducted in a parasitic mode of operation, where SHIP received a smaller portion of the available beam, approximately 10%. The reaction products entered the JetRIS apparatus through a 3.2 μm titanium foil. The highly charged fusion-evaporation products were stopped in the gas and converted to +1 ions through interactions with the argon buffer gas before being transported to the heated filament, where they were neutralized and carried through the de Laval nozzle for subsequent laser spectroscopy in the gas jet.

A two-step laser ionization scheme was used to produce photoions for transport to the silicon detector, with the laser pulses temporally overlapped. The first step was tuned to 333.761 nm to excite the ground state $^1S_0 \leftrightarrow {}^1P_1$ transition [12]. The light was transported to the JetRIS apparatus via optical fiber, and a spherical telescope was used to create a round beam spot with a diameter of approximately 10 mm, antipropagating with the gas jet. This laser was kept at 30 mW with a 15 kHz repetition rate, resulting in an average energy of 2 μJ per pulse. The second step was a nonresonant ionization step provided by the third harmonic of a 15 kHz repetition rate Nd:YAG laser at 355 nm. The second step laser power was kept at 30 W, resulting in an average energy of 2 mJ per pulse. A set of cylindrical telescopes was used to shape the beam into a stripe of 40 mm in width and 4 mm in height, which was injected in a transverse geometry to the jet. The dimensions of the ionization laser beam were chosen based on the repetition rate of the laser and the speed of the gas jet, so that each atom would be irradiated at least once. This specific geometric configuration was chosen to avoid shining the high-power ionization laser through the nozzle and into the gas cell. Heating of the nozzle could change its performance, and the light could potentially damage the thin entrance window separating the gas cell from SHIP. α decays were measured with the PIPS detector as a function of the first step wavelength, with a gate on the known energy of the ^{254}No α decay to avoid any increase in background from long-lived daughters of previously measured isotopes. In addition to the laser spectroscopic measurements, this also provided the first online results for the overall experimental and transport efficiencies, which could be compared to the previously discussed offline studies.

A. Experimental efficiencies

The overall experimental efficiency from the production target to the PIPS detector can be calculated based on the different measurements performed during the experiment. As the overall production and transmission of ^{254}No at SHIP is well known, the transport efficiency from the gas cell to the detector was calculated using "flushing" measurements, where no attracting potential was applied to the neutralizing filament, allowing ions to be transported through the nozzle, captured by the bent RFQ, and implanted on the PIPS detector where the characteristic α-decay was detected. The flushing count rate provides information about the efficiency of the transport of ions through the system, but cannot provide information about the processes in which losses occur, such as neutralization through collisions with the buffer gas, collection and evaporation of neutrals, or their transport through the exit

TABLE I. Experimental efficiencies of the JetRIS apparatus.

Type	Efficiency (%)
Ionization	8.4(2.8)
Transport	0.24(2)
Detection	50
Overall	0.010(3)

channel and the nozzle. The production of ^{254}No is linearly proportional to the primary beam intensity delivered by the UNILAC. Due to changes in the operation of the accelerator, this intensity fluctuated throughout the experiment and was constantly monitored. For a valid comparison of measurements performed at different times throughout the experiment, the count rate was normalized to the integrated primary beam intensity and is reported as a standard Coulomb counter (scc) which is proportional to the beam integral. The flushing measurements were performed intermittently throughout the experiment to monitor the operation of JetRIS. Flushing rates of 1045(25) and 98(20) ions/scc were observed for ^{155}Yb and ^{254}No, respectively. Previous experiments at SHIP have established approximately four ^{254}No ions per second entering the gas cell with a beam intensity of 0.7 particle ·μA, corresponding to a transport efficiency of 0.24(2)% for ^{254}No.

In addition to the flushing measurements, diagnostic laser spectroscopy measurements were performed with ^{155}Yb to check the operation of JetRIS and to determine the ionization efficiency, with the assumption that the behavior of ytterbium and nobelium would be similar as they are chemical homologues with similar atomic transition strengths [12,29]. The laser spectroscopy measurements of ^{155}Yb were performed with a broadband laser to excite the atoms, and only completed once during the online experiment.

The detected ion rate of the laser spectroscopy measurements was compared to the flushing ion rate and used to determine the experimental efficiency of the system. A flushing rate of 1045(25) ions/scc was observed, while the maximum count rate during laser spectroscopy was 45(16) ions/scc. Based on the ratio of the ions observed in the flushing mode of operation to photoions measured during laser spectroscopy, an ionization efficiency of 4(1)% was determined. A similar procedure can be applied to the flushing and maximum count rates from the nobelium measurement, albeit with a larger statistical error. Here the flushing rate of 98(20) ions/scc can be compared to a maximum of the spectrum of 8.4(2.8) ions/scc, resulting in an ionization efficiency of 8.5(3.0)%, agreeing well with the data of Yb and supporting the assumption that the two species have similar behaviors. In sum, the overall efficiency from the above values equates to a 0.010(3)% laser spectroscopy efficiency, shown in comparison with the corresponding contributions in Table I.

Although the experimental efficiency of JetRIS was two orders of magnitude lower than what is typically achieved with RADRIS, there is no inherent reason for the efficiency to be significantly small. New COMSOL simulations are guiding a redesign of the gas cell with the aim of improving the transport efficiency to the 5–10 % level. Initial results indicate that most ions are lost in the transfer from the funnel electrodes to the nozzle. Other work is ongoing to improve the reproducibility of the system, such as a new mounting system for the RFQ to prevent misalignment with the gas jet.

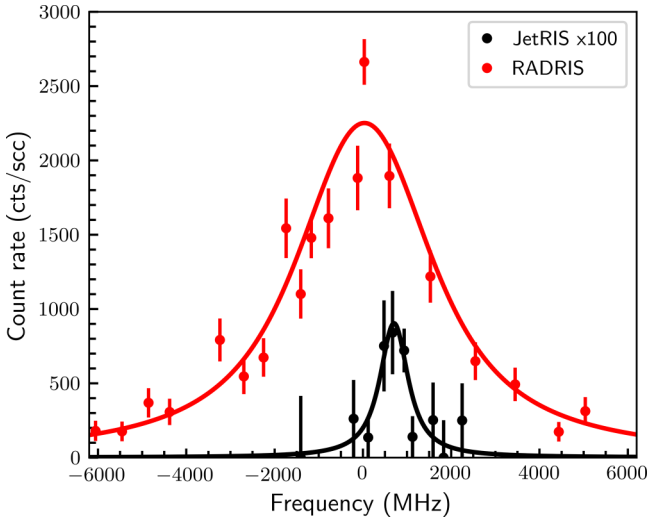

FIG. 9. Measured spectrum of ^{254}No in JetRIS with previous data from RADRIS [11]. The achievable resolution with JetRIS is improved fivefold compared to RADRIS.

B. ^{254}No laser spectroscopy

The main goal of the JetRIS beamtime was the measurement of the $^1S_0 \leftrightarrow {}^1P_1$ transition of the ^{254}No nuclear ground state as a proof of principle that JetRIS is capable of high-resolution measurements of very low production rate nuclides.

The targeted transition of ^{254}No was successfully measured, and is shown in comparison to a previous measurement from the RADRIS experiment [11] in Fig. 9. ^{254}No has nuclear spin $I = 0$, featuring no hyperfine splitting of the transition and thus only one peak was expected.

The spectrum was fit to the data shown in Fig. 9 using most likelihood estimation (MLE) due to the low statistics of the experiment. The fit was performed with raw counts before normalization, while the fit function was scaled per data point according to the relative beam intensity scaling. The fit was performed with an assumption of zero background, with the data gated on α decays within an energy range of 7.93–8.24 MeV. Surface ionization of species from the heated filament has been previously studied at RADRIS [30,31] and is known to be negligible. The centroid resonance frequency of the spectrum was determined to be 29 951.480(2)(10) cm^{-1}, with the statistical and systematic uncertainties shown, respectively. The statistical and systematic contributions to the uncertainty are given separately and will be described in more detail. It is noted that although the overall efficiency of JetRIS is significantly lower than that of RADRIS, the enhancement in precision allows for the extraction of the centroid with a similar statistical uncertainty. The fit resulted in a full width at half-maximum (FWHM) of 770 ± 300 MHz with a G-test score of 0.82. The previously reported measurement of ^{254}No from RADRIS featured a spectral resolution of approximately 3900 MHz [11], demonstrating a factor of 5 improvement in JetRIS.

TABLE II. Contributions to the uncertainty in the centroid frequency of the $^1S_0 \leftrightarrow {}^1P_1$ transition of ^{254}No with JetRIS and RADRIS.

Uncertainty	RADRIS (MHz)	JetRIS (MHz)
Fit	125	60
Wavemeter	150	60
Ne Lamp/HeNe calibration	150	150
Pressure shift	1025	
Doppler shift		150
Total	1350	370

Previous offline measurements of Dy [20] and Cu isotopes achieved a higher resolution, and based on the mass dependence of the Doppler broadening within the gas jet, we expect a spectral resolution of down to 200 MHz for ^{254}No. We believe that our measurement was significantly affected by power broadening. The saturation photon flux for this transition is 2.5×10^{12} photons pulse^{-1} cm^{-2} [11], whereas this measurement used 4.3×10^{12} photons pulse^{-1} cm^{-2}, almost twice the saturation flux. Additionally, previous measurements with Cu isotopes at KU Leuven have shown that saturation conditions in the gas jet are significantly different from those in the gas cell environment, with a tenfold reduction in the saturation flux in the gas jet [24]. Improvements in the overall efficiency of the system will allow lower laser power to be used for the first-step laser excitation, reducing the effect of this broadening.

C. Centroid discrepancy with RADRIS measurements

The centroid of the $^1S_0 \leftrightarrow {}^1P_1$ transition was determined to be 29 961.480(2)(12) cm^{-1}, with a shift of approximately +700 MHz in relation to the previously reported measurement in RADRIS [11]. However, the JetRIS measurement is red Doppler-shifted due to the antipropagating geometry of the first-step laser in relation to the hypersonic flow direction, contributing a shift of 1725(150) MHz. The stagnation temperature, T_0, was assumed to be room temperature as both simulations [19] and offline measurements have established that the stagnation temperature is consistent with room temperature. The uncertainty in the stagnation temperature was conservatively assigned using an upper limit on the temperature established in Ref. [20] using the JetRIS apparatus. In that measurement, a large resistively heated atom source was placed in the mouth of the nozzle, and it is assumed that it induces more heating of the surrounding gas than the thin filament used in the current measurements. After correcting for the Doppler shift, a discrepancy of 2400 MHz is found between the JetRIS and RADRIS data.

The uncertainties considered in this analysis can be seen in Table II. The most significant source of uncertainty results from the unknown pressure shift in the RADRIS data, which was conservatively estimated at −10 MHz/mbar based on previous measurements in thallium [9]. Recent systematic measurements with the wavemeters used in both experiments have revealed further systematic uncertainties. Two different wavemeters of the same model were used for the experiments, both WS7 (HighFinesse) wavemeters, although with separate calibration methods. The JetRIS experiment utilized a frequency-stabilized helium-neon (HeNe) laser for calibration. This HeNe laser features a 150 MHz uncertainty in its wavelength, while the wavemeter boasts a 30 MHz uncertainty in its accuracy. The RADRIS wavemeter relied on an internal neon lamp for calibration, with a 150 MHz uncertainty, although it is possible to calibrate it with an external HeNe laser. Both wavemeters were compared to search for a possible source of the discrepancy in the data by measuring the fundamental and doubled UV light of the pulsed dye amplifier described above. The laser light was coupled to a single-mode fiber with two outputs, allowing for simultaneous measurement of the laser light. The use of a single-mode fiber introduced an additional 30 MHz uncertainty in the measurement of the fundamental light, and subsequently a 60 MHz uncertainty for the doubled laser light. A small difference of 150 MHz was observed between the two wavemeters when using different calibration sources, but this was eliminated by calibration of both wavemeters with the same HeNe laser.

The overall uncertainty in the centroid for each measurement was determined summing in quadrature the statistical error of the fit and the systematic uncertainty introduced by the wavemeters and further summing the systematic uncertainties introduced by the Doppler and pressure shifts. The significance of the discrepancy between the JetRIS and RADRIS centroids rises to the 1.6 σ level. Future measurements are planned to improve our understanding of the systematic uncertainties of both the JetRIS and RADRIS experiments and to resolve this discrepancy. Although challenging in practice, a different geometrical configuration of the lasers, with both propagating transverse to the gas jet, could avoid the Doppler shift and reduce the possible sources of uncertainty in the measurement. It is worth noting that a centroid shift in the JetRIS data stemming from the slip effect, where the seeded heavy mass atoms in the gas jet have a lower velocity in comparison to that of the carrier gas, can be ruled out. Recent measurements were performed at KU Leuven with ^{232}Th atoms seeded in an argon flow to form a gas jet with an identical nozzle and very similar experimental conditions. The results show that ^{232}Th moves in the hypersonic jet at a similar speed to the argon carrier gas [32]. We believe that significant fluctuations in the room temperature of the laser room due to the weather conditions and operation of the laser systems could have introduced a systematic drift in the wavemeter calibration. Additionally, as the pressure shift in the RADRIS data is currently the largest source of the error, future measurements are planned at GSI to measure the ^{254}No spectrum at a range of pressures, allowing for experimental determination of the pressure shift.

V. OUTLOOK

These results are a promising first step towards high-resolution laser spectroscopy measurements of the heavy actinides, allowing for more precise determination of nuclear properties from hyperfine spectra. Current work is focused on improving the experimental efficiency. Additionally, a multireflection time-of-flight (MR-TOF) mass spectrometer is being commissioned for use with JetRIS. The incorporation of the MR-TOF will allow for detection methods beyond

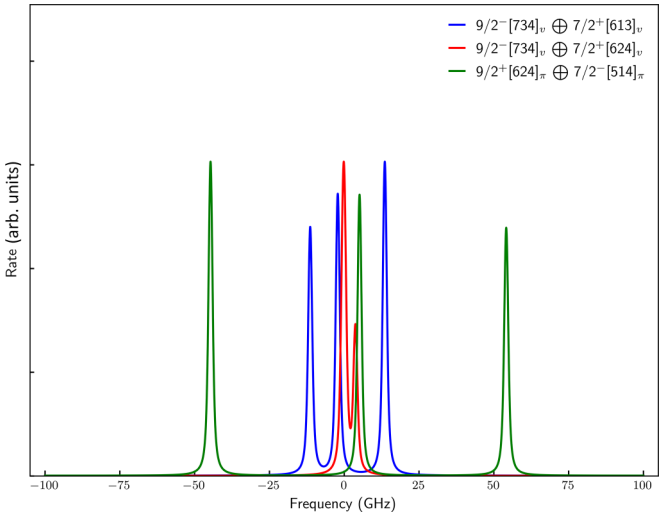

FIG. 10. Hyperfine splitting of the $K = 8^-$ isomer in ^{254}No compared to the nuclear ground state. Three possibilities of the nucleonic configuration are shown, calculated from g_k values provided in Ref. [37], and result in substantially different splittings. The resolution shown here is based on the demonstrated spectral resolution of 770 MHz.

alpha decay, providing access to isotopes or elements with unfavorable decay modes and/or longer half-lives.

With these upgrades, future measurements with the JetRIS apparatus are planned at GSI aiming at nuclides and isomers that feature hyperfine splitting, providing important information about the nuclear structure with higher precision than what is available with the RADRIS technique. Of particular interest is the $K = 8^-$ isomer of ^{254}No, which is populated in approximately 1/3 of the produced ^{254}No nuclei [33]. This high angular momentum isomer was observed in decay spectroscopy studies [33–36], however the configuration of the two-quasiparticle state on which the isomer is based could not be established unambiguously. This isomer has remained out of reach of RADRIS due to its short lifetime ($T_{1/2} \approx 250$ ms). Due to the short lifetime of the isomer in relation to the nuclear ground state, the α-decay energy cannot be used to distinguish the two. However, due to the nonzero nuclear spin, and as each of the possible configurations is predicted to have different g -factors, the hyperfine splitting of each configuration would be sufficiently different that high-resolution laser spectroscopy could both separate the isomer from the nuclear ground state and determine which of the possible configurations is correct. The predicted spectra of the three likely candidates for the configuration in the $K = 8^-$ isomer are shown in Fig. 10 with the demonstrated spectral resolution of JetRIS. The hyperfine spectra were calculated using g_k values predicted from Ref. [37]. It is noted that there is a possible overlap between the resonance of the $K = 8^-$ isomer and the nuclear ground state, meaning that a contribution by the $K = 8^-$ isomer to the spectral broadening and discrepancy in the centroid frequency discussed is possible. However, based on the production rate of the isomer and the transport time through the JetRIS apparatus, the contribution would be rather small. Additionally, the above calculations do not account for the isomer shift between the ground state and the $K = 8^-$ isomer, which, based on other isomers in heavy nuclei, could rise to the level of hundreds of MHz [38,39]. However, we cannot fully exclude the possibility of the presence of the isomer in our measurements, and future measurements will clarify the situation.

VI. CONCLUSION

An apparatus utilizing the in-gas-jet laser ionization spectroscopy technique was successfully characterized offline and commissioned for online studies of heavy actinides at GSI. This apparatus combines the efficient RADRIS technique of heated filament neutralization with the in-gas-jet resonant ionization spectroscopy technique to provide high sensitivity with high resolution. Offline characterization was performed with stable and radioactive sources to understand the capabilities of the system as well as the optimal operating parameters. An online experiment was performed at GSI, where a sub-GHz laser spectroscopic measurement of ^{254}No was performed, with a fivefold improvement in the resolution over existing measurements. This improvement in the spectral resolution opens the door for high-resolution measurements in the heavy actinide region, providing information on the nuclear structure with high precision, which is critical for benchmarking nuclear theory. New technical improvements are being incorporated to improve the performance of JetRIS, such as a multireflection time-of-flight mass spectrometer and changes in the design of the gas cell to improve the efficiency. This work will open opportunities to access new elements, isotopes, and isomers in the heavy actinide region.

ACKNOWLEDGMENTS

We would like to thank Dr. Dennis Renisch at the Johannes Gutenberg University of Mainz for providing the ^{223}Ra recoil source used for the commissioning work. The online measurements presented here were performed at the velocity filter SHIP at the GSI Helmholtzzentrum für Schwerionenforschung, Darmstadt (Germany) in the frame of FAIR Phase-0 (Experiment U321). We would also like to thank the GSI ion source and accelerator staff for providing intense ion beams. This project has received funding from the European Union's Horizon 2020 research and innovation programme under Grant Agreement No. 861198-LISA-H2020-MSCA-ITN-2019. M.L., E.K., and E.R.-R. acknowledge funding from the European Research Council (ERC) under the European Union's Horizon 2020 research and innovation programme (Grant Agreement No. 819957). P.C. acknowledges the European Union's Horizon 2020 research and innovation programme under the Marie Skłodowska-Curie Grant Agreement No. 101026762. This work has received funding from the German Bundesministerium für Bildung und Forschung (BMBF, Germany) under Project No. 05P21UMFN3 and the Research Foundation Flanders (FWO, Belgium) BOF KU Leuven (C14/22/104) and the FWO and F.R.S.-FNRS under the Excellence of Science (EOS) program (40007501). T.W. acknowledges funding from the Bundesministerium für Bildung und Forschung (BMBF, Germany) under Grants No. 05P15RDFN1 and No. 05P21RDFN1.

[1] B. Cheal and K. T. Flanagan, Progress in laser spectroscopy at radioactive ion beam facilities, J. Phys. G **37**, 113101 (2010).

[2] P. Campbell, I. Moore, and M. Pearson, Laser spectroscopy for nuclear structure physics, Prog. Part. Nucl. Phys. **86**, 127 (2016).

[3] W. Nörtershäuser, New developments in laser spectroscopy for ribs, Int. School Phys. Enrico Fermi **201**, 293 (2019).

[4] M. Block, M. Laatiaoui, and S. Raeder, Recent progress in laser spectroscopy of the actinides, Prog. Part. Nucl. Phys. **116**, 103834 (2021).

[5] X. Yang, S. Wang, S. Wilkins, and R. G. Ruiz, Laser spectroscopy for the study of exotic nuclei, Prog. Part. Nucl. Phys. **129**, 104005 (2023).

[6] H. Backe, M. Hies, H. Kunz, W. Lauth, O. Curtze, P. Schwamb, M. Sewtz, W. Theobald, R. Zahn, K. Eberhardt, N. Trautmann, D. Habs, R. Repnow, and B. Fricke, Isotope shift measurements for superdeformed fission isomeric states, Phys. Rev. Lett. **80**, 920 (1998).

[7] M. Sewtz, H. Backe, A. Dretzke, G. Kube, W. Lauth, P. Schwamb, K. Eberhardt, C. Grüning, P. Thörle, N. Trautmann, P. Kunz, J. Lassen, G. Passler, C. Z. Dong, S. Fritzsche, and R. G. Haire, First observation of atomic levels for the element fermium ($Z = 100$), Phys. Rev. Lett. **90**, 163002 (2003).

[8] C. Granados, P. Creemers, R. Ferrer, L. P. Gaffney, W. Gins, R. de Groote, M. Huyse, Y. Kudryavtsev, Y. Martínez, S. Raeder, S. Sels, C. Van Beveren, P. Van den Bergh, P. Van Duppen, K. Wrzosek-Lipska, A. Zadvornaya, A. E. Barzakh, B. Bastin, P. Delahaye, L. Hijazi *et al.*, In-gas laser ionization and spectroscopy of actinium isotopes near the $N = 126$ closed shell, Phys. Rev. C **96**, 054331 (2017).

[9] W. Lauth, H. Backe, M. Dahlinger, I. Klaft, P. Schwamb, G. Schwickert, N. Trautmann, and U. Othmer, Resonance ionization spectroscopy in a buffer gas cell with radioactive decay detection, demonstrated using ^{208}Tl, Phys. Rev. Lett. **68**, 1675 (1992).

[10] H. Backe, W. Lauth, M. Block, and M. Laatiaoui, Prospects for laser spectroscopy, ion chemistry and mobility measurements of superheavy elements in buffer-gas traps, Nucl. Phys. A **944**, 492 (2015).

[11] M. Laatiaoui, W. Lauth, H. Backe, M. Block, D. Ackermann, B. Cheal, P. Chhetri, Ch. E. Düllmann, P. Van Duppen, J. Even, R. Ferrer, F. Giacoppo, S. Götz, F. P. Heßberger, M. Huyse, O. Kaleja, J. Khuyagbaatar, P. Kunz, F. Lautenschläger, A. K. Mistry *et al.*, Atom-at-a-time laser resonance ionization spectroscopy of nobelium, Nature (London) **538**, 495 (2016).

[12] F. Lautenschläger, P. Chhetri, D. Ackermann, H. Backe, M. Block, B. Cheal, A. Clark, C. Droese, R. Ferrer, F. Giacoppo, S. Götz, F. Heßberger, O. Kaleja, J. Khuyagbaatar, P. Kunz, A. Mistry, M. Laatiaoui, W. Lauth, S. Raeder, T. Walther *et al.*, Developments for resonance ionization laser spectroscopy of the heaviest elements at SHIP, Nucl. Instrum. Methods Phys. Res. Sect. B **383**, 115 (2016).

[13] S. Raeder, D. Ackermann, H. Backe, R. Beerwerth, J. C. Berengut, M. Block, A. Borschevsky, B. Cheal, P. Chhetri, Ch. E. Düllmann, V. A. Dzuba, E. Eliav, J. Even, R. Ferrer, V. V. Flambaum, S. Fritzsche, F. Giacoppo, S. Götz, F. P. Heßberger, M. Huyse *et al.*, Probing sizes and shapes of nobelium isotopes by laser spectroscopy, Phys. Rev. Lett. **120**, 232503 (2018).

[14] P. Chhetri, D. Ackermann, H. Backe, M. Block, B. Cheal, C. Droese, Ch. E. Düllmann, J. Even, R. Ferrer, F. Giacoppo, S. Götz, F. P. Heßberger, M. Huyse, O. Kaleja, J. Khuyagbaatar, P. Kunz, M. Laatiaoui, F. Lautenschläger, W. Lauth, N. Lecesne *et al.*, Precision measurement of the first ionization potential of nobelium, Phys. Rev. Lett. **120**, 263003 (2018).

[15] J. Warbinek, B. Anđelić, M. Block, P. Chhetri, A. Claessens, R. Ferrer, F. Giacoppo, O. Kaleja, T. Kieck, E. Kim, M. Laatiaoui, J. Lantis, A. Mistry, D. Münzberg, S. Nothhelfer, S. Raeder, E. Rey-Herme, E. Rickert, J. Romans, E. Romero-Romero *et al.*, Advancing radiation-detected resonance ionization towards heavier elements and more exotic nuclides, Atoms **10**, 41 (2022).

[16] Y. Kudryavtsev, R. Ferrer, M. Huyse, P. Van den Bergh, and P. Van Duppen, The in-gas-jet laser ion source: Resonance ionization spectroscopy of radioactive atoms in supersonic gas jets, Nucl. Instrum. Methods Phys. Res. Sect. B **297**, 7 (2013).

[17] S. Raeder, B. Bastin, M. Block, P. Creemers, P. Delahaye, R. Ferrer, X. Fléchard, S. Franchoo, L. Ghys, L. Gaffney, C. Granados, R. Heinke, L. Hijazi, M. Huyse, T. Kron, Y. Kudryavtsev, M. Laatiaoui, N. Lecesne, F. Luton, I. Moore *et al.*, Developments towards in-gas-jet laser spectroscopy studies of actinium isotopes at LISOL, Nucl. Instrum. Methods Phys. Res. Sect. B **376**, 382 (2016).

[18] R. Ferrer, A. Barzakh, B. Bastin, R. Beerwerth, M. Block, P. Creemers, H. Grawe, R. de Groote, P. Delahaye, X. Fléchard, S. Franchoo, S. Fritzsche, L. P. Gaffney, L. Ghys, W. Gins, C. Granados, R. Heinke, L. Hijazi, M. Huyse, T. Kron *et al.*, Towards high-resolution laser ionization spectroscopy of the heaviest elements in supersonic gas jet expansion, Nat. Commun. **8**, 14520 (2017).

[19] S. Raeder, M. Block, P. Chhetri, R. Ferrer, S. Kraemer, T. Kron, M. Laatiaoui, S. Nothhelfer, F. Schneider, P. Van Duppen, M. Verlinde, E. Verstraelen, T. Walther, and A. Zadvornaya, A gas-jet apparatus for high-resolution laser spectroscopy on the heaviest elements at SHIP, Nucl. Instrum. Methods Phys. Res. Sect. B **463**, 272 (2020).

[20] D. Münzberg, M. Block, A. Claessens, R. Ferrer, M. Laatiaoui, J. Lantis, S. Nothhelfer, S. Raeder, and P. Van Duppen, Resolution characterizations of JetRIS in Mainz using ^{164}Dy, Atoms **10**, 57 (2022).

[21] G. Münzenberg, W. Faust, S. Hofmann, P. Armbruster, K. Güttner, and H. Ewald, The velocity filter SHIP, a separator of unslowed heavy ion fusion products, Nucl. Instrum. Methods **161**, 65 (1979).

[22] M. Block, F. Giacoppo, F.-P. Heßberger, and S. Raeder, Recent progress in experiments on the heaviest nuclides at SHIP, Riv. Nuovo Cimento **45**, 279 (2022).

[23] R. Ferrer, M. Verlinde, E. Verstraelen, A. Claessens, M. Huyse, S. Kraemer, Y. Kudryavtsev, J. Romans, P. Van den Bergh, P. Van Duppen, A. Zadvornaya, O. Chazot, G. Grossir, V. I. Kalikmanov, M. Nabuurs, and D. Reynaerts, Hypersonic nozzle for laser-spectroscopy studies at 17 K characterized by resonance-ionization-spectroscopy-based flow mapping, Phys. Rev. Res. **3**, 043041 (2021).

[24] E. Verstraelen, Laser Spectroscopy of Actinides: Octupole Deformation and Gas-Jet Characterization, Ph.D. thesis, KU Leuven (2021).

[25] A. Zadvornaya, P. Creemers, K. Dockx, R. Ferrer, L. P. Gaffney, W. Gins, C. Granados, M. Huyse, Y. Kudryavtsev, M. Laatiaoui, E. Mogilevskiy, S. Raeder, S. Sels, P. Van den Bergh, P. Van Duppen, M. Verlinde, E. Verstraelen, M. Nabuurs,

D. Reynaerts, and P. Papadakis, Characterization of supersonic gas jets for high-resolution laser ionization spectroscopy of heavy elements, Phys. Rev. X **8**, 041008 (2018).

[26] M. Verlinde, R. Ferrer, A. Claessens, C. A. Granados, S. Kraemer, Y. Kudryavtsev, D. Li, P. Van den Bergh, P. Van Duppen, and E. Verstraelen, Single-longitudinal-mode pumped pulsed-dye amplifier for high-resolution laser spectroscopy, Rev. Sci. Instrum. **91**, 103002 (2020).

[27] O. Kaleja, B. Anđelić, K. Blaum, M. Block, P. Chhetri, C. Droese, Ch. E. Düllmann, M. Eibach, S. Eliseev, J. Even, S. Götz, F. Giacoppo, N. Kalantar-Nayestanaki, M. Laatiaoui, E. M. Ramirez, A. Mistry, T. Murböck, S. Raeder, L. Schweikhard, and P. Thirolf, The performance of the cryogenic buffer-gas stopping cell of SHIPTRAP, Nucl. Instrum. Methods Phys. Res. Sect. B **463**, 280 (2020).

[28] Y. T. Oganessian, V. K. Utyonkov, Y. V. Lobanov, F. S. Abdullin, A. N. Polyakov, I. V. Shirokovsky, Y. S. Tsyganov, A. N. Mezentsev, S. Iliev, V. G. Subbotin, A. M. Sukhov, K. Subotic, O. V. Ivanov, A. N. Voinov, V. I. Zagrebaev, K. J. Moody, J. F. Wild, N. J. Stoyer, M. A. Stoyer, and R. W. Lougheed, Measurements of cross sections for the fusion-evaporation reactions ^{204,206,207,208}Pb + ^{48}Ca and ^{207}Pb + ^{34}S : decay properties of the even-even nuclides ^{238}Cf and ^{250}No, Phys. Rev. C **64**, 054606 (2001).

[29] W. F. Meggers, C. H. Corliss, and B. F. Scribner, Natl. Bur. Stand. (US), Monogr. **145**, 292 (1975).

[30] M. Laatiaoui, H. Backe, M. Block, F.-P. Heßberger, P. Kunz, F. Lautenschläger, W. Lauth, M. Sewtz, and T. Walther, On laser spectroscopy of the element nobelium (zÂ =Â 102), Eur. Phys. J. D **68**, 71 (2014).

[31] T. Murböck, S. Raeder, P. Chhetri, K. Diaz, M. Laatiaoui, F. Giacoppo, and M. Block, Filament studies for laser spectroscopy on lawrencium, Hyperfine Interact. **241**, 35 (2020).

[32] A. Claessens, Laser ionization spectroscopy of ^{254}No and ^{229}Th in hypersonic gas jets, Ph.D. thesis, KU Leuven (2024).

[33] F. P. Heßberger, S. Antalic, B. Sulignano, D. Ackermann, S. Heinz, S. Hofmann, B. Kindler, J. Khuyagbaatar, I. Kojouharov, P. Kuusiniemi, M. Leino, B. Lommel, R. Mann, K. Nishio, A. G. Popeko, Š. Šáro, B. Streicher, J. Uusitalo, M. Venhart, and A. V. Yeremin, Decay studies of *K* isomers in ^{254}No, Eur. Phys. J. A **43**, 55 (2010).

[34] A. Ghiorso, K. Eskola, P. Eskola, and M. Nurmia, Isomeric states in ^{250}Fm and ^{254}No, Phys. Rev. C **7**, 2032 (1973).

[35] S. K. Tandel, T. L. Khoo, D. Seweryniak, G. Mukherjee, I. Ahmad, B. Back, R. Blinstrup, M. P. Carpenter, J. Chapman, P. Chowdhury, C. N. Davids, A. A. Hecht, A. Heinz, P. Ikin, R. V. F. Janssens, F. G. Kondev, T. Lauritsen, C. J. Lister, E. F. Moore, D. Peterson *et al.*, K isomers in ^{254}No : Probing single-particle energies and pairing strengths in the heaviest nuclei, Phys. Rev. Lett. **97**, 082502 (2006).

[36] R. Clark, K. Gregorich, J. Berryman, M. Ali, J. Allmond, C. Beausang, M. Cromaz, M. Deleplanque, I. Dragojević, J. Dvorak, P. Ellison, P. Fallon, M. Garcia, J. Gates, S. Gros, H. Jeppesen, D. Kaji, I. Lee, A. Macchiavelli, K. Morimoto *et al.*, High-K multi-quasiparticle states in ^{254}No, Phys. Lett. B **690**, 19 (2010).

[37] R. D. Herzberg, P. T. Greenlees, P. A. Butler, G. D. Jones, I. G. Darby, S. Eeckhaudt, T. Grahn, C. Gray-Jones, F. P. Hessberger, and P. JonesIsomer spectroscopy of ^{254}No, Phys. Scr. **T125**, 73 (2006).

[38] K. M. Lynch, J. Billowes, M. L. Bissell, I. Budinčević, T. E. Cocolios, R. P. De Groote, S. De Schepper, V. N. Fedosseev, K. T. Flanagan, S. Franchoo, R. F. Garcia Ruiz, H. Heylen, B. A. Marsh, G. Neyens, T. J. Procter, R. E. Rossel, S. Rothe, I. Strashnov, H. H. Stroke, and K. D. A. Wendt, Decay-assisted laser spectroscopy of neutron-deficient francium, Phys. Rev. X **4**, 011055 (2014).

[39] J. G. Cubiss, A. E. Barzakh, M. D. Seliverstov, A. N. Andreyev, B. Andel, S. Antalic, P. Ascher, D. Atanasov, D. Beck, J. Biero, K. Blaum, C. Borgmann, M. Breitenfeldt, L. Capponi, T. E. Cocolios, T. Day Goodacre, X. Derkx, H. De Witte, J. Elseviers, D. V. Fedorov *et al.*, Charge radii and electromagnetic moments of $^{195-211}$at, Phys. Rev. C **97**, 054327 (2018).